Langmuir

Article

pubs.acs.org/Langmuir

Investigation of Halide-Induced Aggregation of Au Nanoparticles into Spongelike Gold

Zhiqiang Zhang,*[,†] Haiwen Li,[†] Feng Zhang,[§] Yihui Wu,[‡] Zhen Guo,[†] Lianqun Zhou,[†] and Jiadong Li[§]

[†]Suzhou Institute of Biomedical Engineering and Technology, Chinese Academy of Sciences, Suzhou 215163, PR China

[§]Suzhou Institute of Nano-tech and Nano-bionics, Chinese Academy of Sciences, Suzhou 215123, PR China

[‡]State Key Laboratory of Applied Optics, Changchun Institute of Optics, Fine Mechanics and Physics, Chinese Academy of Sciences, Changchun 130033, PR China

Supporting Information

ABSTRACT: We present a facile method for fabricating spongelike Au structures by halide-induced aggregation and fusion of gold nanoparticles (AuNPs). Halide ions (F^-, Cl^-, Br^-, and I^-) showed distinctly different effects on the synthesized AuNPs, which were characterized by localized surface plasmon resonance (LSPR) and dynamic light scattering measurements. A noticeable red-shift in the LSPR peak was found after Br^- and I^- ion treatment, which indicates the adsorption of halide atoms or ions on the AuNPs. The surface potential of AuNPs varied by treatment with different types of halides; this finding indicates that different halide ions have different effects on the AuNPs. Br^- and I^- ions showed strong affinity toward the AuNPs. The different affinities of halide ions toward the AuNPs play an important role in controlling the formation process of spongelike gold. Citrate ions adsorbed on AuNPs were displaced by halide ions to different extents. Such displacement determined the aggregation and fusion behaviors of the AuNPs and eventually the formation of different spongelike structures.

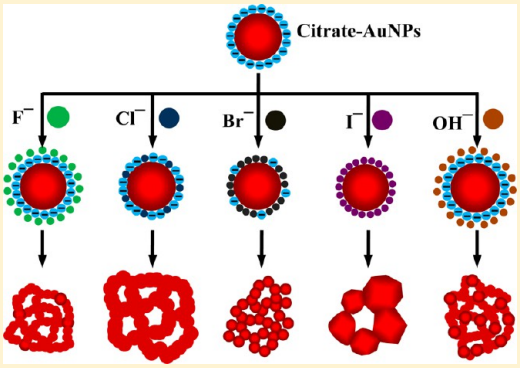

INTRODUCTION

Nanoporous gold (spongelike gold) with three-dimensional networked porous architectures has attracted considerable attention in recent years.[1−4] Spongelike gold has a wide range of applications in catalysis,[5−7] fuel cells,[8−10] electrochemistry,[11,12] biosensors,[13,14] and actuators.[15,16] The general approaches to fabricate such a functional nanomaterial include dealloying of Au−M alloy (M = Ag,[17−19] Cu,[20,21] and Al[22]), templating methods using soft and hard materials,[23−26] and electro-polymerization of Au nanoparticles.[27−30] In these methods, some procedures such as strong acid or high-temperature treatment are required to remove the sacrificial metal or organic templates. These processes may raising environmental problems, and the final compositions of formed gold sponge cannot be well-controlled, which plays an important role in their applications such as catalysis or biosensing.[31] Therefore, some new approaches have been developed to fabricate such gold porous nanostructures.[32,33] Self-assembly is a facile route to form spongelike nanostructures from single gold nanoparticles.[31,34] By this approach, however, it still remains a challenge to control the size of the ligaments and pores of the gold sponge through a one-step process under moderate manners.

Previous studies have confirmed that halide ions have different affinity for metal surfaces.[35] The degree of specific adsorption on a metal surface increases in the order $F^- < Cl^- < Br^- < I^-$, indicating the decreasing energy of solvation of these species. Specially, F^- has the lowest affinity and only nonspecifically or weakly specifically adsorbs on metal surface. Cl^-, Br^-, and I^- can chemisorb on the gold surface to form a Au−X bond with an increasingly covalent character in the order Cl < Br < I.[36−38] The halide ions have been used as additives that greatly affect the size and shape of synthesized gold nanoparticles.[39−41] Many investigations have shown that the addition of Br^- or I^- will displace the stabilizer on gold nanoparticles (AuNPs) and result in aggregation and fusion of the AuNPs to form anisotropic nanocrystals.[42,43] For example, the addition of KI into colloidal AuNPs leads to the effect of electron donation, which results in fusion/fragmentation of AuNPs.[42] Also, spongelike gold nanocomposites formed after addition of NaBr into an amino acid stabilized AuNPs sol.[44] However, other types of halide ions are seldom reported to have the ability to generate spongelike structures, and the effect of halide ions on the aggregation of colloidal AuNPs is also not well-known.

Here, we studied the effect of four types of halide ions on the aggregation of the citrate-capped AuNPs and demonstrated that Au spongelike architectures were obtained after addition of halides into AuNPs of three different sizes. The halide ions with different affinities toward the AuNPs resulted in spongelike

Received: December 2, 2013
Revised: February 18, 2014
Published: February 20, 2014

   dx.doi.org/10.1021/la4046447 | Langmuir 2014, 30, 2648−2659

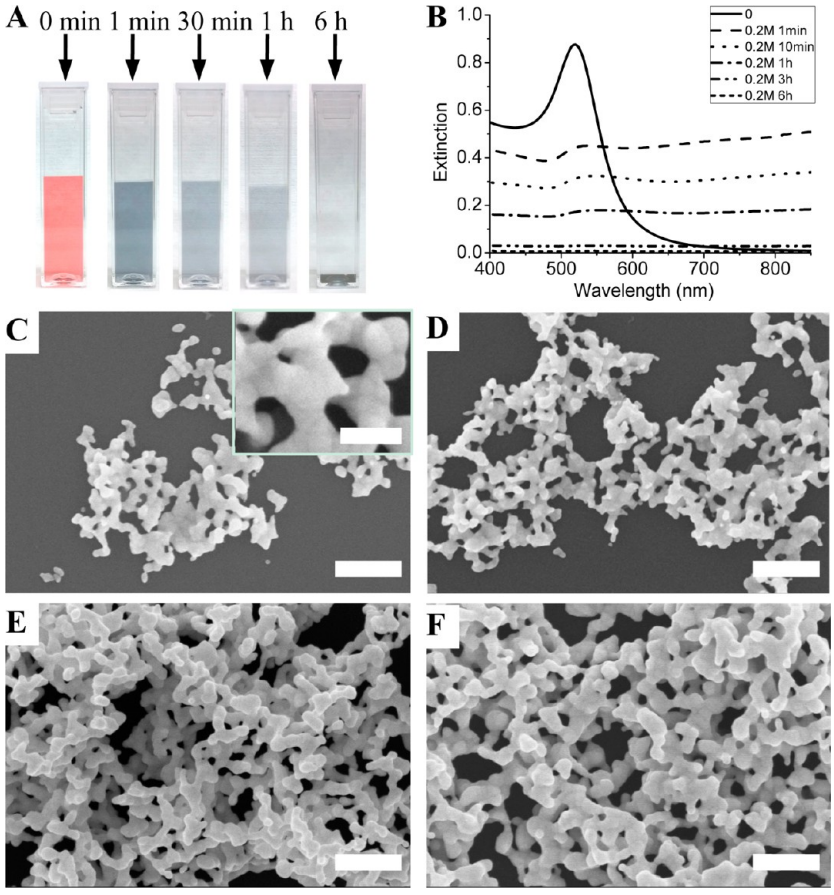

Figure 1. Induced aggregation of colloidal gold nanoparticles by 0.18 M NaCl. (A) UV−vis extinction spectrum of the AuNPs sols after addition of 0.18 M NaCl within 6 h. (B) Color changes in the AuNPs sols after addition of 0.18 M NaCl within 6 h. SEM images of NaCl-induced aggregated AuNPs obtained after (C) 10 min, (D) 30 min, (E) 1 h, and (F) 6 h. The inset in part C shows a high-magnification image of the AuNPs. The scale bars in parts C−F indicate 400 nm, and the scale bar in the inset in C indicates 100 nm.

gold with different morphologies. The localized surface plasmon resonance (LSPR) change of AuNPs showed that addition of NaBr and NaI induced a red-shift in the resonance peak, indicating the adsorption of the halide atoms. The dynamic light scattering (DLS) measurements showed that the surface potential of AuNPs varied by treating with different types of halides, indicating the different effects of halide ions on the AuNPs. The NaX-induced formation of spongelike gold has potential applications in catalysis and surface-enhanced Raman scattering (SERS) as well as biological detection.

EXPERIMENTAL METHODS

Materials. Hydrogen tetrachloroaurate ($HAuCl_4{\cdot}4H_2O$, >99.9%), NaF, NaCl, NaBr, NaI, NaOH, and trisodium citrate ($C_6H_5O_7Na_3{\cdot}2H_2O$) were purchased from Sinopharm Chemical Reagent Co. Ltd. (Shanghai, China) and used without further purification. Milli-Q H_2O (18.2 $M\Omega{\cdot}cm^{-1}$) was used for all experiments. All other reagents were of analytical grade.

Synthesis of Citrate-Capped AuNPs. Aqueous suspensions of citrate-stabilized 18,, 35, and 65 nm AuNPs were prepared using the Frens method.[45,46] Briefly, 200 mL of 0.01% (w/v) $HAuCl_4$ solution was heated to boiling under vigorous stirring with refluxing. After 1 min, 8, 3, and 2.4 mL of 1% (w/v) sodium citrate, respectively, was rapidly added to the boiling solution, and the mixture was allowed to boil for 20 min. The prepared gold colloids were then cooled to room temperature with constant stirring and stored at 4 °C in a dark bottle. To avoid any possible effect of residual ions in the as-prepared AuNPs solution on the halide-induced aggregation of AuNPs, a certain volume of AuNPs was concentrated by centrifugation at 9000 rpm for 15 min and redispersed in the same volume pure water. Care was taken to ensure that the supernatants were completely removed without disturbing the concentrated AuNPs. All glassware was rigorously cleaned in aqua regia (3:1 HCl:HNO_3) and rinsed thoroughly with Milli-Q H_2O before use.

The Au molar concentration in the18, 35, and 65 nm AuNPs was 0.24 mM. The concentration of gold NPs was calculated to be 1.3 nM (7.6×10^{11} NPs/mL) for the 18 nm AuNPs, 0.17 nM (1.0×10^{11} NPs/mL) for the 35 nm AuNPs, and 0.027 nM (1.6×10^{10} NPs/mL) for the 65 nm AuNPs by assuming that all added Au^{3+} ions were reduced to Au^0 atoms by citrate in solution and formed spherical AuNPs. The citrate concentrations in the synthesized AuNPs solutions were 1.3 mM for the 18 nm AuNPs, 0.5 mM for the 35 nm AuNPs, and 0.4 mM for the 65 nm AuNPs.

Gold Sponge Formation. The spongelike gold formed in a standard quartz cuvette with a 1 cm optical path length. After added 2 mL of AuNPs solution into the cuvtte, 0.2 mL of 2 M NaF, NaCl, NaBr, and NaI solution were added. Afterward, the (3-aminopropyl)-triethoxysilane (APTES) functionalized silicon substrates (APTES-Si) with a 6 mm^2 size were immersed into the mixture, and they were left without any disturbance to allow the spongelike gold to deposit on the APTES-Si substrates. After various times, the APTES-Si substrates were taken out and were rinsed with pure water and ethanol several times and dried in air. These samples were stored in N_2 atmosphere for catalytic reaction and SERS measurement.

Preparation of APTES-Derivatized Substrates. The glass or silicon (Si) slides were cleaned in piranha solution (7:3 H_2SO_4:H_2O_2) at 120 °C for 20 min, rinsed thoroughly with distilled water, and dried using pure N_2 flow, in accordance with a previous method.[47] ***Caution!*** *Piranha solution is very corrosive and must be handled with extreme care.*

dx.doi.org/10.1021/la4046447 | *Langmuir* 2014, 30, 2648−2659

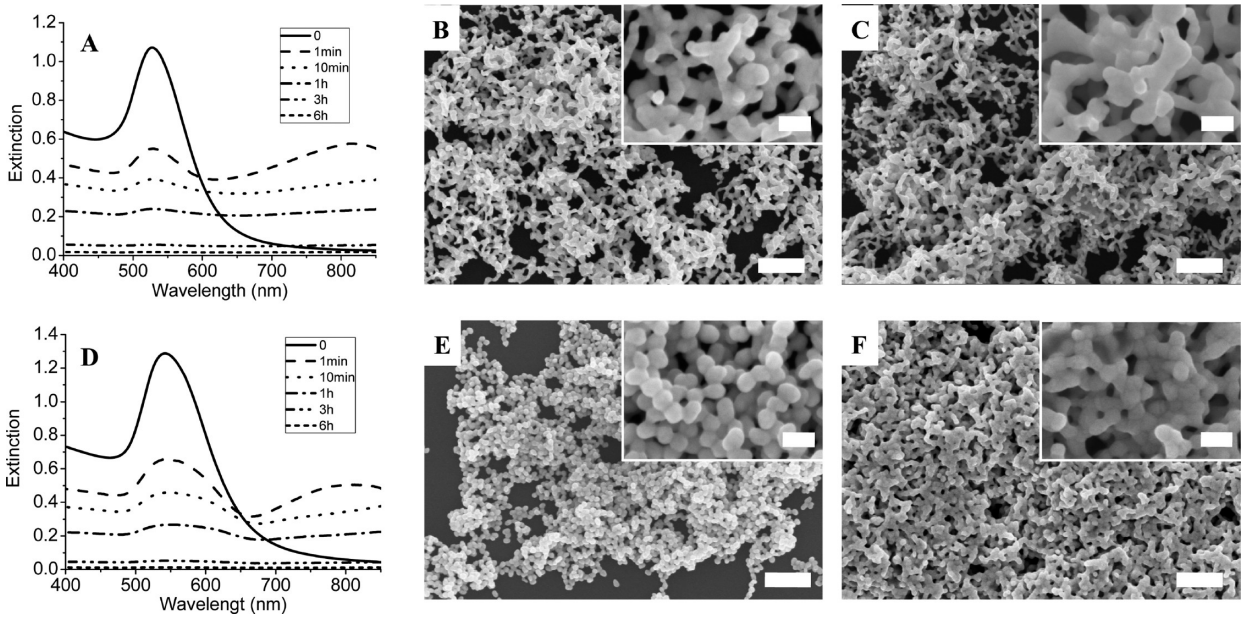

Figure 2. UV−vis extinction spectrum and the SEM images of 0.18 M NaCl-induced aggregation of 35 and 65 nm gold nanoparticles: (A−C) 30 nm AuNPs, (D−F) 60 nm AuNPs, (B, E) aging time of 1 h, and (C, F) aging time of 6 h. The scale bars indicate 500 nm, and the scale bar in the inset indicates 100 nm.

After rinsing with methanol for 5 min, the substrates were immersed in 5% (v/v) APTES in methanol for 1 h and rinsed five times in methanol for 10 min, followed by deionized water to hydrolyze the residual ethoxy functionalities for 30 min. The slides were then dried using pure N_2 flow at 120 °C for 1 h to promote silane cross-linkage. The APTES-derivatized glass or Si slides (designated as NH_2/SiO_2) were stored in a desiccator for further use.

NaX Treatment of AuNPs in Solution and Immobilized AuNPs Submonolayer. NaX (12 mM) was added to the AuNPs solutions, and UV−vis spectra were obtained after 5 min. The NH_2/SiO_2 substrates were immersed in AuNPs solutions for 12 h to form the AuNP submonolayer and then rinsed with Milli-Q H_2O to remove the unbound AuNPs. The AuNP monolayer was then immersed in 0.18 M NaX solution for 20 min, followed by rinsing with Milli-Q water, and the UV−vis spectra of the AuNPs in water were measured. The calculated values of used halide ions to the total surface areas of the AuNPs were 1.4×10^5 ions/nm^2 for the 18 nm AuNPs, 2.7×10^5 ions/nm^2 for the 35 nm AuNPs, and 5.0×10^5 ions/nm^2 for the 65 nm AuNPs.

Characterization Methods. All UV−vis extinction spectra were measured using a Perkin-Elmer Lambda 950 UV/vis/NIR spectrophotometer. The morphologies of the NP assemblies formed were characterized using a Hitachi S-4800 field-emission scanning electron microscope (FE-SEM) at 10 kV. Zeta potential and size of the AuNPs were measured by a Malvern Zetasizer Nano-ZS90 at 25.0 ± 0.1 °C, and the surface potential fitting model was the Smoluchowski model.

RESULTS AND DISCUSSION

NaCl-Induced Aggregation of 18 nm AuNPs. Colloidal gold nanoparticles are stable in solution because the citrate capping layer of the AuNPs provides an electrostatic repulsion force resulting from the electric double layer.[48,49] Moreover, the force of the electric double layer (EDL) greatly depends on the ionic strength of the solution, which is closely related to the Debye length of the EDL.[50,51] It is well-known that the addition of excessive salt into the gold sol could cause the aggregation of the AuNPs, with the color changing from ruby red to blue. The NaCl-induced aggregation of colloidal AuNPs has been used as an analytic tool for detection of DNA, thrombin, melamine, and heavy metal ions.[52−54] Therefore, NaCl was first chosen for the study of halide-induced aggregation of AuNPs.

After addition of 0.18 M NaCl, the color of the AuNP sol turns from ruby red to blue immediately. By further extending the aging time to 6 h, the solution became colorless, accompanied with sedimentation at the bottom of cuvette (Figure 1A). The color change of the AuNP solution was monitored by UV−vis extinction spectra (Figure 1B). The extinction maximum peak (λ_{max}) showed a red-shift from 518 to 540 nm after addition of 0.18 M NaCl and became broad during the reaction. The intensity of the λ_{max} at about 518 nm decreased while the absorption in the near-IR region increased with the time. The flattened shape of the optical spectrum above 600 nm indicates the formation of network aggregation.[55] As shown in the SEM images of aggregation at different aging times (Figure 1C−F), the 3D spongelike structures consist of fused interconnected nanowires with the mean diameter of 100 nm that formed after the addition of 0.18 M NaCl. The elemental analysis shows that the composition of the formed spongelike structures is gold (Supporting Information, Figure S1). The formation of spongelike structures starts to take place at about 10 min, and stable gold sponge is formed within 6 h, which can be indirectly traced by the decreased level of the optical spectrum of the solution during the reaction. As shown in the inset image in Figure 1C, the boundaries can be clearly indentified in the nanowires formed after the aging time of 10 min, and these boundaries were still shown in the final gold sponge (Supporting Information, Figure S2). It is clear that the final gold sponge results from the gradually further aggregation and fusion of the smaller spongelike structures formed at 10 min.

To know the size effect of the AuNPs on the dynamics of formation of gold sponge, 0.18 M NaCl was added in the 35 and 65 nm AuNPs solution. The extinction spectrum and the SEM images of three differently sized AuNPs used in this study are shown in Figure S3 (Supporting Information). For the 35 nm AuNPs, the position of λ_{max} at about 528 nm just red-shift

dx.doi.org/10.1021/la4046447 | Langmuir 2014, 30, 2648−2659

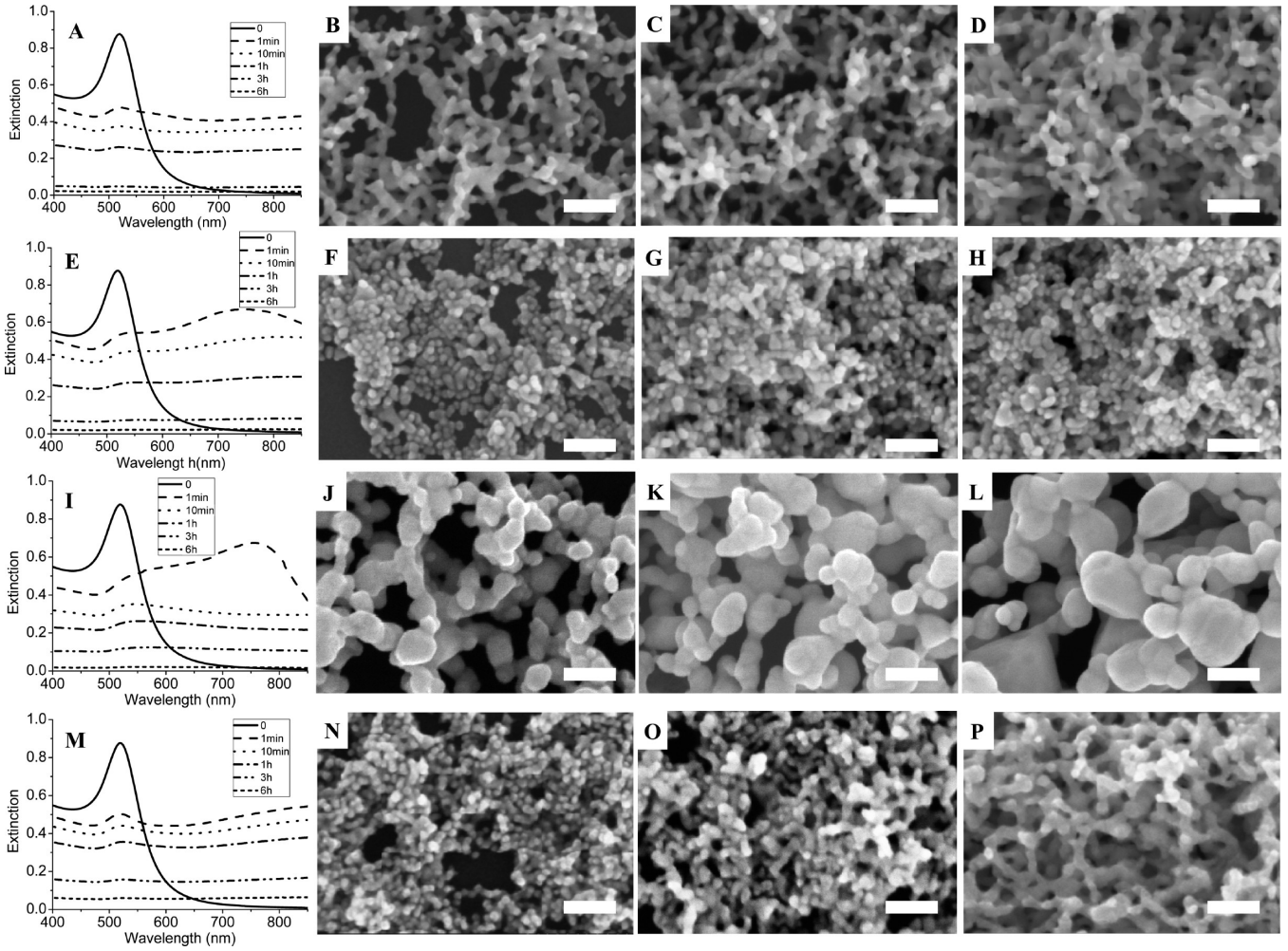

Figure 3. Gold sponge induced by addition of 0.18 M (A–D) NaF, (E–H) NaBr, (I–L) NaI, and (M–P) NaOH. The aging time: (B, F, J, N) 10 min, (C, G, K, O) 1 h, and (D, H, L, P) 6 h. All scale bars indicate 100 nm.

about two nanometer after addition of 0.18 M NaCl (Figure 2A), which is much smaller than the 18 nm AuNPs at the same salt concentration. Meanwhile, a new extinction peak at about 820 nm appeared and it became broad and disappeared at longer aging time. For the 65 nm AuNPs, the same trend was found in its optical spectrum after 0.18 M NaCl treatment. The position of the extinction peak showed a red-shift from 540 to 554 nm after addition of 0.18 M NaCl. Also, a second extinction peak at about 810 nm appeared after addition of NaCl and became broad as the aging time increases. The difference in optical extinction under the same condition between the two large AuNPs and the 18 nm AuNPs indicates the different dynamics of aggregation of the AuNPs. This prediction was verified by the SEM images of formed gold sponge (Figure 2B,C,E,F). As shown, the speed of formation of gold sponge for the 35 nm AuNPs is slower than that for the 18 nm AuNPs, and that of the 65 nm AuNPs is slower than that of the 35 nm AuNPs. This can be judged from the morphologies of the formed gold sponge after the same aging time. That is, the size of nanowires at the aging time of 1 h in the 35 nm AuNPs system is smaller than that at the aging time of 6 h. For the 65 nm AuNPs system, AuNPs formed 3D network aggregation without fusion at the aging time of 1 h; however, gold sponge formed after 6 h of aging time. There is another difference in the formation of gold sponge between small AuNPs and large ones, that is, the large-sized AuNPs tended to form much compacted gold sponge but with a slower formation speed. These different behaviors in the formation of gold sponge for differently sized AuNPs may contribute to the lower diffusion rate of large nanoparticles in solution and lower reactivity of the naonparticle due to the size effect.

NaF-, NaBr-, and NaI-Induced Aggregation of 18 nm AuNPs. AuNPs solution was treated with three different halide ions and one non-halide ion (OH^-), as shown in Figure.3. For NaF (Figure 3A–D), the shape of the optical spectra at above 600 nm after addition of the salt became flattened, which is similar to the NaCl case. At the aging time of 10 min, the nanowires in formed spongelike structure have the diameter from 20 to 60 nm, and it clearly shows that there are many nodes in the nanowires. The spongelike structures became more compact with the aging time increases. For NaBr (Figure 3E–H), AuNPs tend to form a close, compact structure, which is similar to the aggregation induced by 36 mM NaCl. For NaI (Figure 3J–L), a spongelike structure with the nodes' size greater than 100 nm formed, and the average feature size increased to 200 nm with the aging time of 6 h. The different formation of spongelike structures between NaI and other halide salts was also shown in its optical spectra after addition of NaI salt (Figure 3I). NaOH was used for comparing the different response of AuNPs between the halide salts and non-

dx.doi.org/10.1021/la4046447 | *Langmuir* 2014, 30, 2648–2659

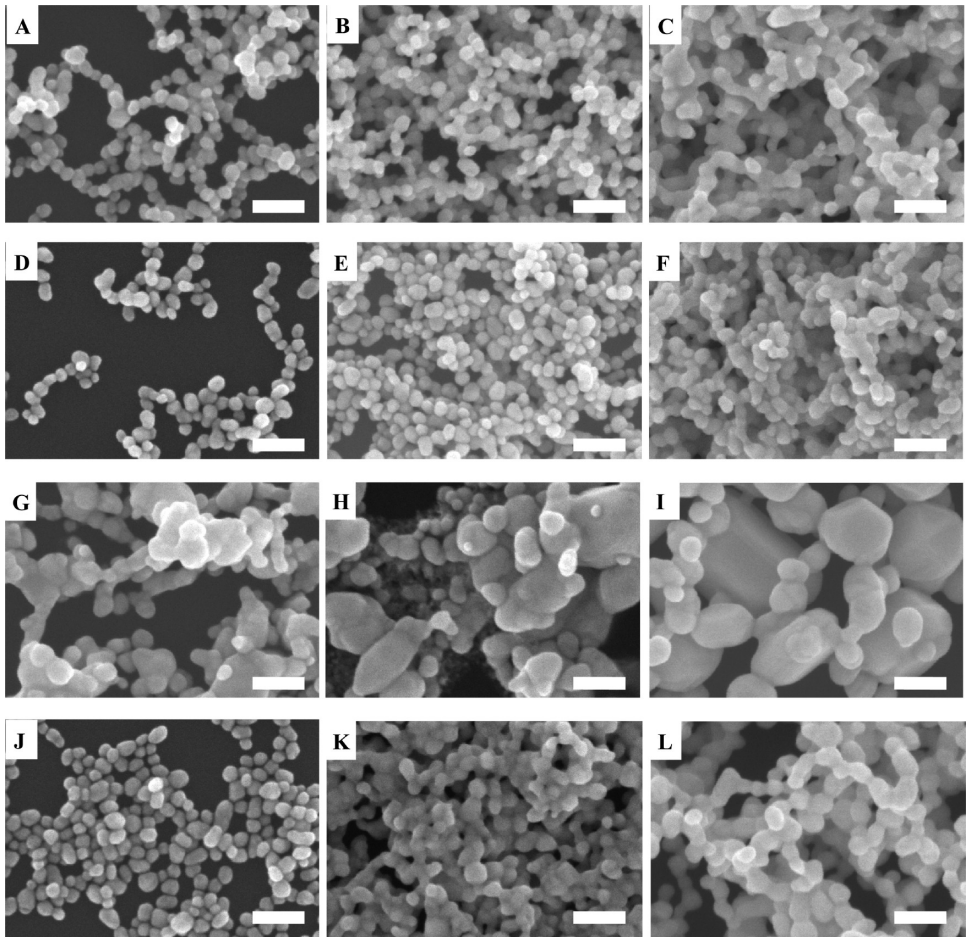

Figure 4. NaX-induced gold sponge for 35 nm AuNPs. (A–C) NaF, (D–F) NaBr, (G–I) NaI, and (J–L) NaOH. The aging time: (A, D, G, J) 10 min, (B, E, H, K) 1 h, and (C, F, I, L) 6 h. All scale bars indicate 100 nm.

halide salt. As shown in Figure 3M–P, the formation process of spongelike structures induced by NaOH is between those of NaF and NaBr.

NaX-Induced Spongelike Gold for 35 and 65 nm AuNPs. To explore the size effect of AuNPs on the NaX-induced spongelike aggregation, citrate-capped AuNPs with the diameter of 35 and 65 nm were treated with halide salts, as shown in Figures 4 and 5, respectively. For the 35 nm AuNPs (Figure 4), the formation of spongelike structures is slower than that of the 18 nm AuNPs. It clearly shows that the coalescence of nanowires in spongelike structures is greatly reduced for all NaX, salts except for NaCl. The similar trend was also shown for 65 nm AuNPs (Figure 5). Specially, the treatment of NaI just resulted in a few submicrometer particles after the 6 h aging time. However, the production of submicrometer particles induced by NaI was found in the 10-fold concentrated 65 nm AuNPs solution, as shown in Figure S4 (Supporting Information). The effect of concentration of AuNPs on the formation of spongelike structures was not shown for other NaX salts (data not shown).

Effect of F^-, Cl^-, Br^-, and I^- on AuNPs. The localized surface plasmon resonance (LSPR)[56] of the AuNPs was used to study the effect of halide ions on the AuNPs because the LSPR is very sensitive to the size, shape, interparticle distance, free electron density, and surrounding medium.[57] The LSPR peak is described[58] by $\lambda_{sp} = 2\pi c[(\varepsilon_0 m_e(\varepsilon_\infty + \kappa n_m^2))/(Ne^2)]^{1/2}$, where ε_∞ is the high-frequency contribution to the dielectric function, ε_0 is the permittivity of free space, m_e is the effective electron mass, N is the electron density of the metal, n_m is the medium refractive index, and κ is the nanoparticle geometry-dependent factor ($\kappa = 2$ for a sphere).

According to the theory of stability of colloidal nanoparticles,[48,49] the ionic strength of 12 mM cannot induce aggregation of the AuNPs,[59] and the AuNPs tend to aggregate at the ionic strength above 24 mM (Supporting Information, Figure S5). Therefore, the 12 mM halide salts were choose for LSPR peak monitoring first. For 18 nm AuNPs, the LSPR peak showed noticeable red-shift after treatment with 12 mM NaBr and a blue-shift upon treatment with 12 mM NaOH, as shown in Figure 6A, while the extinction band around 600 nm rose up after Br^- and I^- treatment. These trends in spectrum change induced by halide ions decreased as the size of AuNPs increases, as shown in Figure 6B and 6C for 35 and 65 nm AuNPs, respectively. The LSPR peak shift of the AuNPs after 12 mM NaX salts treatment are summarized in Figure 6D. Previous studies have shown that iodine atoms will form a monolayer spontaneously on a bulk gold surface in dilute iodide solution.[60] Additionally, the extra electrons could inject into the AuNPs generated by the reductive chemisorption of iodine ions in the form of $I^- - e^- \rightarrow I_{(adsorbed)} + e^-$.[61] The electron injection into AuNPs will result in a blue-shift of the LSPR peak.[62] The red-shift of the LSPR peak induced by Br^- and I^- for all AuNPs could be attributed to the formation of Br and I atoms on the surface of AuNPs,[42] in which the change of

dx.doi.org/10.1021/la4046447 | *Langmuir* 2014, 30, 2648–2659

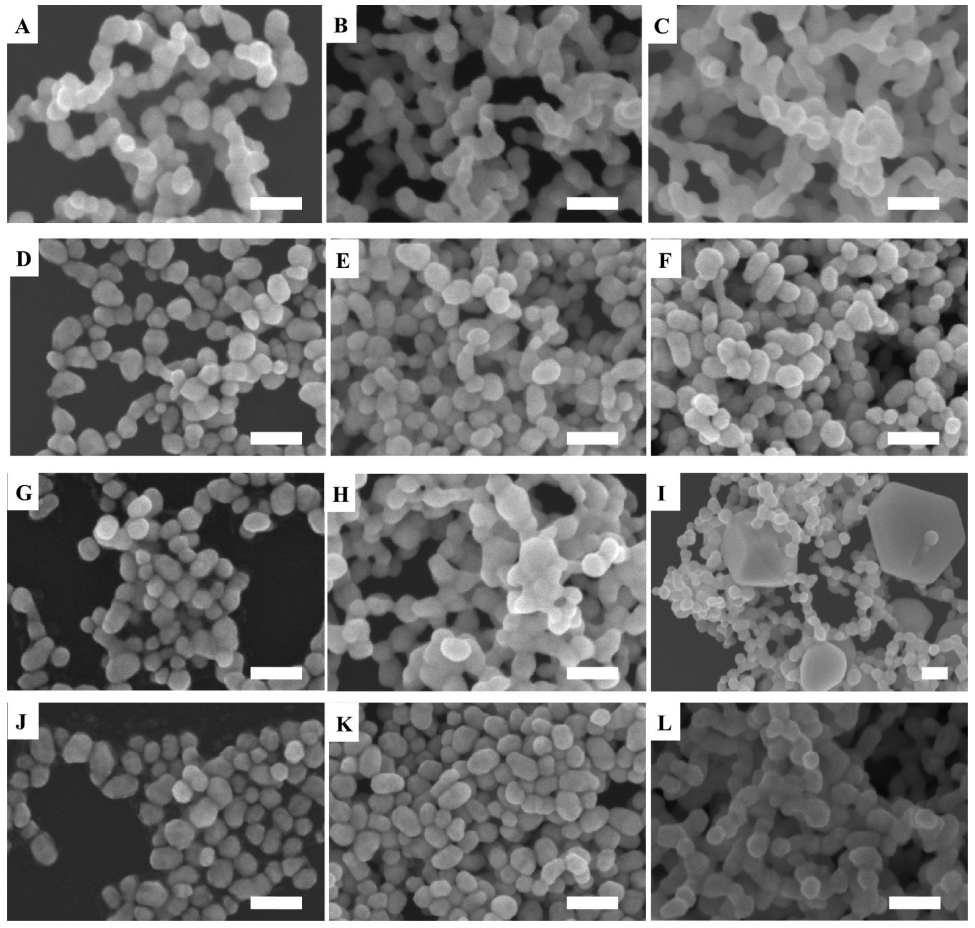

Figure 5. NaX-induced gold sponge for 65 nm AuNPs. (A–C) NaF, (D–F) NaBr, (G–I) NaI, and (J–L) NaOH. The aging time:(A, D, G, J) 10 min, (B, E, H, K) 1 h, and (C, F, I, L) 6 h. All scale bars are 100 nm.

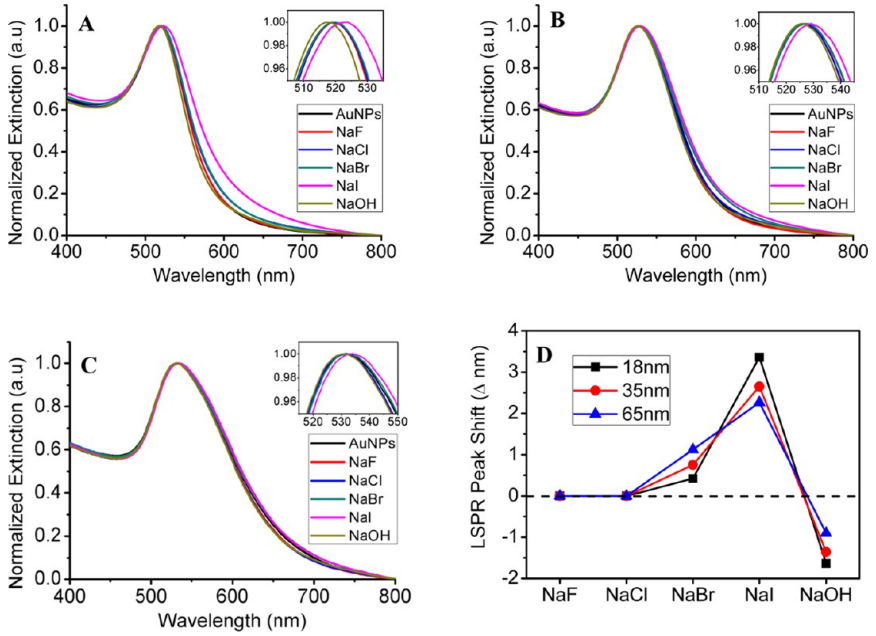

Figure 6. The effect of 12 mM NaX salts on the UV–vis spectrum of AuNPs solution samples: (A) 18 nm AuNPs, (B) 35 nm AuNPs, and (C) 65 nm AuNPs. (D) The LSPR peak shift of three kinds of AuNPs upon treating with NaX salts. The insets in parts A–C indicate the amplified spectrum at the LSPR peak.

n_m of the AuNPs is greater than the N by electron injection. The blue-shift of the LSPR peak induced by NaOH for all AuNPs may contribute to the increase of electron density of the AuNPs,[59] which were injected from the excess electrons

dx.doi.org/10.1021/la4046447 | Langmuir 2014, 30, 2648–2659

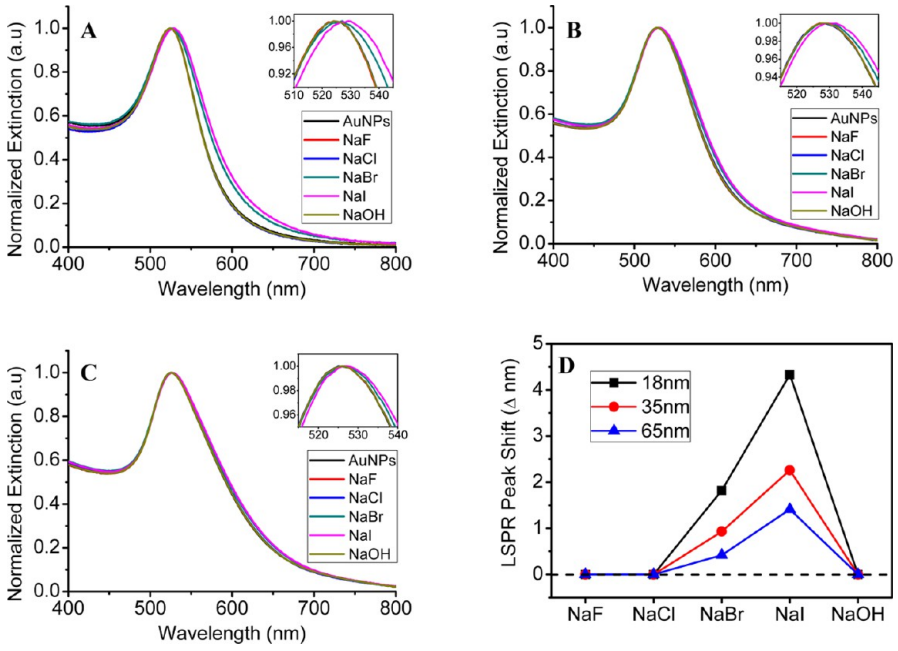

Figure 7. The effect of 0.18 M NaX salts on the UV−vis spectrum of immobilized AuNPs samples: (A) 18 nm AuNPs, (B) 35 nm AuNPs, and (C) 65 nm AuNPs. (D) the LSPR peak shift of three kinds of AuNPs by treating with NaX salts. The insets in parts A−C indicate the amplified spectrum at the LSPR peak.

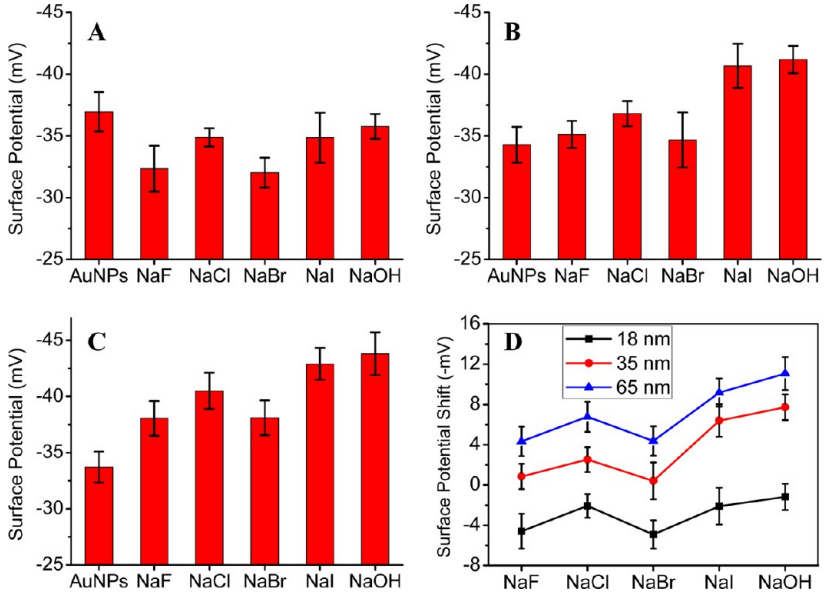

Figure 8. Surface potentials of AuNPs solutions before and after treated with 12 mM NaX salts: (A) 18 nm AuNPs, (B) 35 nm AuNPs, and (C) 65 nm AuNPs. (D) Zeta-potential shift in three different-sized AuNPs after treated with 12 mM NaX salts.

resulting from further ionization of COOH groups on AuNPs in higher pH suspension.

To study the effect of NaX salts with 0.18 M on the AuNPs and to confirm the NaOH-induced blue-shift of AuNPs, the immobilized AuNPs on the glass substrate (AuNPs/NH_2/glass) were used. For the 18 nm AuNPs, the LSPR peak (λ_{max}) showed noticeable red-shift after treatment with 0.18 M NaBr and NaI, as shown in Figure 7A. Also, the extinction band around 600 nm rose up after Br^- and I^- treatment. Similar to treatment with 12 mM NaX salts, the trends in spectrum change induced by 0.18 M halide salts decreased as the size of the AuNPs increases, as shown in Figure 7B,C. The LSPR peak shifts of the AuNPs after treatment with 0.18 M NaX salts are summarized in Figure 7D. The red-shift of the LSPR peak for 18 nm AuNPs can reach up to 4.3 nm for NaI and 1.8 nm for NaBr, which are larger than that of the 12 mM NaX salt treatment (3.4 nm for NaI and 0.4 nm for NaBr). The nonlinear increase of the red-shift of the LSPR peak induced by 15 times higher salt concentrations indicates that the Br and I atoms adsorbed on AuNPs saturated at a concentration lower than 0.18 M.

Dynamic Light Scattering (DLS) Measurements. To further understand the effect of halide ions on the AuNPs, dynamic light scattering was used to measure the surface potential of AuNPs (Figure 8) and size monitoring (Figure 9). For citrate-capped colloidal gold, the surface charge depends on

dx.doi.org/10.1021/la4046447 | *Langmuir* 2014, 30, 2648−2659

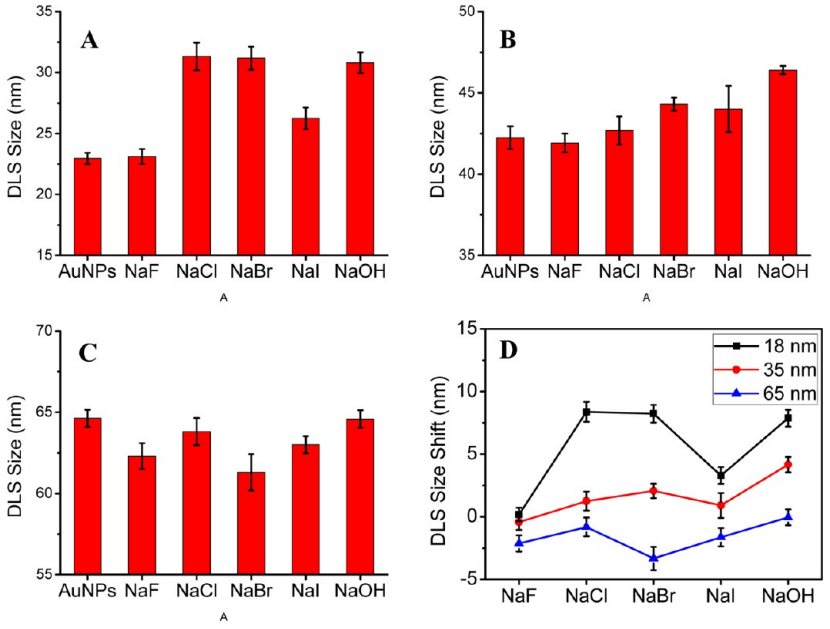

Figure 9. DLS sizes of AuNPs solution before and after treatment with 12 mM NaX salts: (A) 18 nm AuNPs, (B) 35 nm AuNPs, and (C) 65 nm AuNPs. (D) Measured DLS size shifts of three different-sized AuNPs after treated with 12 mM NaX salts.

the degree of ionization of COOH groups of citrates on AuNPs and, hence, the pH of the suspension. As shown in Figure 8A–C, the zeta-potential after addition of 12 mM NaX decreased for 18 nm AuNPs and increased for 35 and 65 nm AuNPs. The change in surface potential after NaX salt treatment for three different-sized AuNPs showed similar trends, as shown in Figure 8D. For 35 and 65 nm AuNPs, 12 mM NaI and NaOH resulted in the largest increase in surface potential among all the NaX salts. The increase of surface potential by NaOH could contribute to the further ionization of the carboxylic groups, which generates more negative charge on AuNPs. For the NaI-induced increase of surface potential, the extra electrons injected in AuNPs may increase the negative charges surrounding the AuNPs. However, for 18 nm AuNPs, addition of NaI and NaOH just led to a little decrease in surface potential. According to the LSPR shift in Figure 6D, the NaI resulted in a 3.4 nm red-shift of the LSPR peak. The differences in surface potential changes of AuNPs with different size under the same treatment condition could attribute to the size effect of nanoparticles, which means that it is related to the ratio of adsorbed iodine atoms to the surface area of AuNPs.

According to the recipe for synthesis of AuNPs, the citrate concentration in synthesized AuNPs solutions are 1.3 mM for the 18 nm AuNPs, 0.5 mM for the 35 nm AuNPs, and 0.4 mM for the 65 nm AuNPs. However, the citrate concentrations in the AuNPs solution decreased because of its consumption in the reduction of Au ions to Au atoms and its role as capping molecules on the AuNPs. Even so, the residual citrate ions in the solutions are adequate to stabilize the AuNPs. In this case, the surface coverage of citrate in different-sized AuNPs varied because of the well-known Langmuir adsorption isotherm. The difference in surface coverage of citrate on different-sized AuNPs was also verified by the zeta-potentials of different-sized AuNPs in Figure 8. The zeta-potentials of larger-sized AuNPs with lower citrate concentrations were lower than those of smaller-sized AuNPs, which is attributed to the lower surface coverage of citrate ions on larger-sized AuNPs.

The size changes measured by DLS showed that the effect of 12 mM NaX salts on 18 nm AuNPs is more significant than for larger AuNPs, as shown in Figure 9. From another point of view, similar trends were found in the measurements of both LSPR (Figure 6A–C) and DLS data for different-sized AuNPs under NaX salt treatment, which indicates the complementary role of LSPR and DLS in monitoring the effect of halide ions. The DLS measured size change induced by halide salts may also be seen from the slight increase in extinction band around 600 nm.

The zeta-potential and size data of the AuNPs obtained by DLS measurements did not show significant trends induced by 12 mM halide ions. To investigate the influence of low ionic strength halide salts on the AuNPs further, we inspected the morphologies of the AuNPs after addition of 12 mM halide salts, as shown in Figure 10. The APTES-functionalized silicon slides (NH_2/Si) were immersed in the AuNP solutions after addition of NaX salts. The AuNPs immobilized on the NH_2/Si

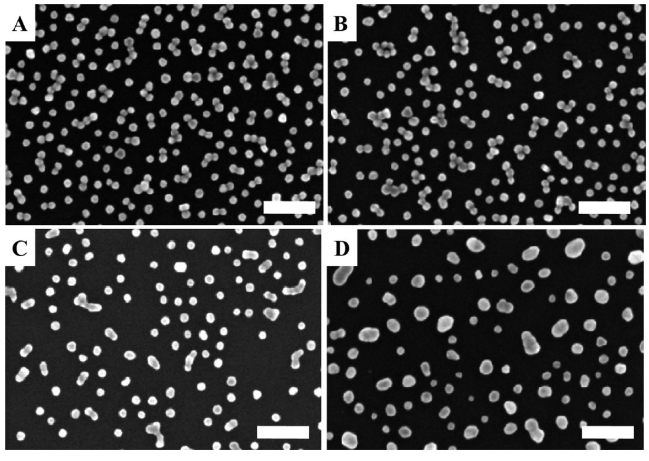

Figure 10. SEM images of 18 nm AuNPs after addition of 12 mM halide salts within 1 h: (A) NaF, (B) NaCl, (C) NaBr, and (D) NaI. All scale bars indicate 100 nm.

dx.doi.org/10.1021/la4046447 | *Langmuir* 2014, 30, 2648–2659

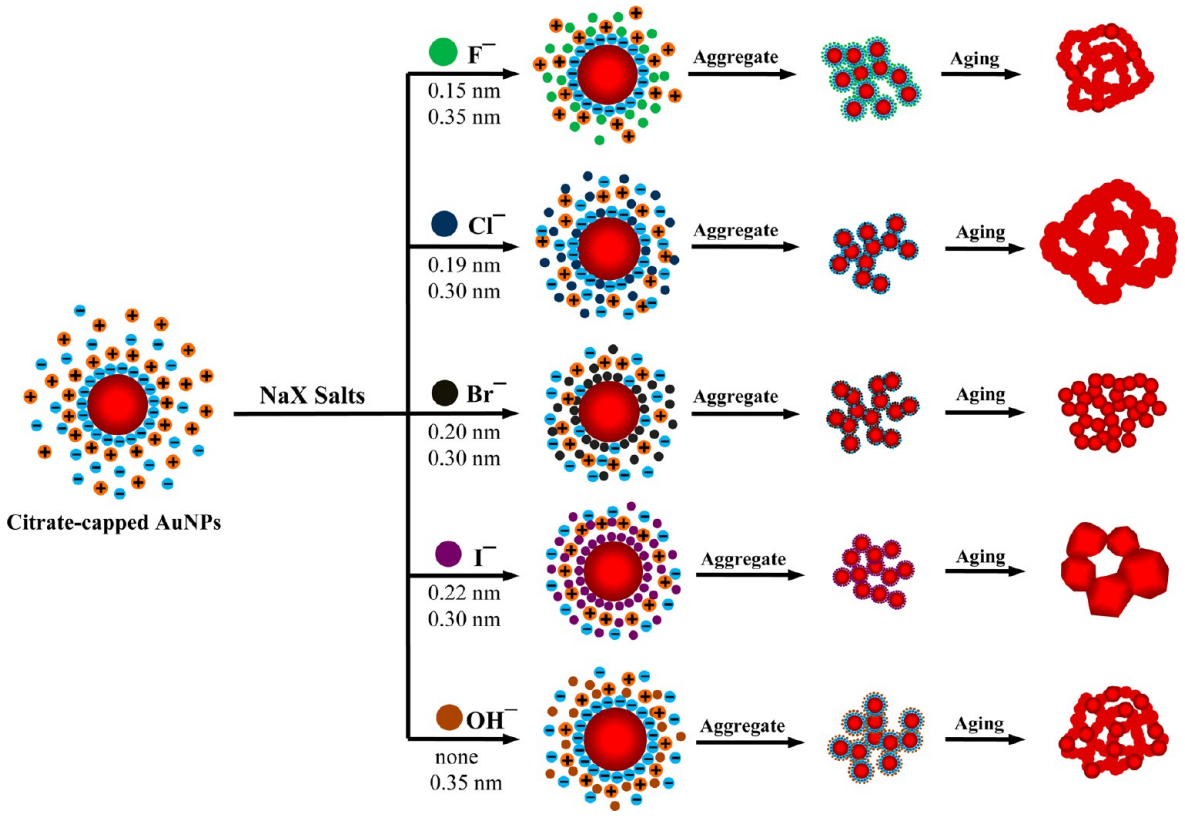

Figure 11. Effects of halide ions on the AuNPs and formation of spongelike gold nanostructures. The two numbers shown under each X^- ion represent the effective diameter of unhydrated (first value) and hydrated (second value) ions extracted from Kielland,[63] and the size of hydrated citrate ion is 0.5 nm.

substrates because of electrostatic attractive forces between negatively charged AuNPs and positively charged APTES on the silicon substrates. In the 18 nm AuNPs, for example, aggregates consisting of several AuNPs formed by addition of NaF and NaCl at the ionic strength of 12 mM. The AuNPs in aggregates induced by NaF and NaCl clearly showed close contact between NPs. By contrast, AuNPs in aggregates induced by NaBr showed some fusion between NPs. After NaI treatment, both small- and large-sized AuNPs formed on the silicon substrate. The increase and decrease in size of the AuNPs induced by NaI can be attributed to the aggregation/fragmentation/fusion effect of iodine.[42] The distinct effect of iodide ions is significant for 18 nm AuNP under low NaI concentrations. However, this effect is weak in the 35 and 65 nm AuNPs, as shown in Figure S6 (Supporting Information). Therefore, the different effects of halide ions on DLS zeta-potential and size measurements may be attributed to the size effects of the NPs.

Halide-Induced Formation of Spongelike Gold. Some earlier studies have shown that halide ions have different affinity for metal surfaces, with the degree of specific adsorption on the metal surface increasing in the order $F^- < Cl^- < Br^- < I^-$.[35] Cl^-, Br^-, and I^- can chemisorb on a gold surface to form a Au−X bond with an increasingly covalent character in the order Cl < Br < I.[36−38] The above LSPR and DLS data also have clearly shown that the Br^- and I^- ions have stronger affinity to citrate-capped AuNPs than other types of X^- ions. The difference in morphologies of spongelike structures induced by four types of halide ions and one non-halide ion indicates the different effects of five types of X^- ions on AuNPs.

On the basis of these experimental results and the previous studies, the mechanism of halide-induced aggregation of AuNPs into spongelike gold structures is given in Figure 11. One effect of addition of 0.18 M NaX salts is to greatly screen the electric double layer of colloidal AuNPs due to the salt effects according to the DLVO theory.[48−51] The effective diameter of unhydrated and hydrated X^- ions defined by a previous study[63] are listed in Figure 11. Besides the effect described above, halide ions also displace the citrate ions adsorbed on the AuNPs. The degree of adsorption of halide ions on AuNPs depends on its affinity for gold. For F^- ions, they cannot replace the citrate ions because of their weak affinity for gold and just provide a salts effect on aggregation of AuNPs. In this case, the electrostatic repulsion between AuNPs is totally screened, and the AuNPs aggregate into three-dimensional networked structures by the driving force of van der Waals attraction. By aging, the nanowires in aggregated networked structures undergo fusion by salt effects, and finally, the spongelike structures formed. Similarly, for Cl^- ions, they may replace some few citrate ions and finally produce spongelike structures with larger-sized nanowires. For Br^- and I^- ions, they will replace much more citrate ions than Cl^- ions. The Br^- ions partially coated AuNPs, forming close-packed aggregation with little fusion, which indicates that the layer of adsorbed Br atoms or Br^- ions prevents the fusion of aggregated structure. The I^- ions have the most distinct effect on aggregation of AuNPs, by which the larger-sized AuNPs with irregular shape are produced. The drastic effect of iodide ions on reshaping the aggregates of AuNPs can be attributed to the well-known etching effect of iodide on gold.[41,64] The specific adsorption of iodine on the surface of AuNPs increases with increasing van der Waals attractive forces,[42] leading to

dx.doi.org/10.1021/la4046447 | Langmuir 2014, 30, 2648−2659

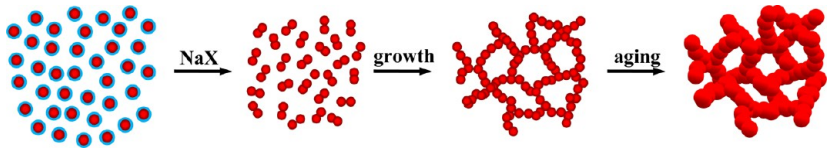

Figure 12. Schematic illustration of the formation process of the spongelike aggregates.

increases in the surface stress of aggregated AuNP structures due to the mismatch between iodine and Au(111).[65] These changes in turn result in reshaping of the AuNP aggregates into larger- or smaller-sized irregular nanoparticles, such as quasi-spherical particles and plates, due to Ostwald ripening.[42] For OH^- ions, it has another effect on AuNPs, which increases the pH of the suspension. This difference induces a little difference in the formation process of spongelike structures. Therefore, the different effects of X^- ions on AuNPs influence the aggregation and fusion of AuNPs and eventually the formation of different spongelike structures.

Mechanism of NaX-Induced Spongelike Aggregation. The colloidal nanoparticles are stable under low ionic strength because of the electrostatic repulsion force between NPs. For monodispersed spherical NPs, the total interaction potential, V_T, is sum of the electrostatic repulsive potential (V_{elec}) and van der Waals attractive potential (V_{vdW}) according to DLVO theory.[48−51]

$$V_T(r) = V_{elec}(r) + V_{vdW}(r) \quad (1)$$

$$V_{elec}(r) = 2\pi\varepsilon_s\varepsilon_0 a\psi_0^{\,2} \ln[1 + \exp(-\kappa H)] \quad \text{if } \kappa a > 5 \quad (2)$$

$$V_{elec}(r) = 4\pi\varepsilon_s\varepsilon_0 a^2 Y^2 \left(\frac{k_B T}{e}\right)^2 \frac{\exp(-\kappa H)}{r} \quad \text{if } \kappa a < 5 \quad (3)$$

$$Y = \frac{8\tanh(e\psi_0/4k_BT)}{1 + \left[1 - \frac{2\kappa a + 1}{(\kappa a + 1)^2}\tanh^2(e\psi_0/4k_BT)\right]^{1/2}} \quad (4)$$

$$\kappa = \left[\frac{1000e^2 N_A(2I)}{\varepsilon_s\varepsilon_0 k_B T}\right]^{1/2} \quad (5)$$

$$V_{vdW}(r) = -\frac{A_H}{6}\left[\frac{2}{R^2 - 4} + \frac{2}{R^2} + \ln\frac{R^2 - 4}{R^2}\right] \quad (6)$$

where r is the center-to-center distance of neighboring NPs of radius a ($R = r/a$), H is the distance of closet approach ($r = H + 2a$), ε_s is the relative dielectric constant of the solvent (about 80 for water), ε_0 is the dielectric constant of vacuum, Ψ_0 is the surface potential of NPs, κ is the inverse Debye length ($\kappa^{-1} = 0.304/[\text{ionic strength}]^{1/2}$ nm for 1:1 electrolytes), and A_H is the Hamaker constant of the particles (2.5×10^{-19} J). The value of surface potential is related the amount of surface charges which could be obtained by several ways, preferential adsorption of ions, dissociation of surface groups, isomorphic substitution, adsorption of polyelectrolytes, and accumulation of electrons. For citrated-stabilized NPs, the surface negative charges are generated from deprotonated −COOH groups in citrate ions.

The formation of spongelike aggregations of AuNPs can be described by the diffusion-limited cluster aggregation model.[66] The surface potential of AuNPs greatly decreased after addition of 0.18 M NaX salts because of the high ionic strength of the solution. Therefore, the van der Waals attractive potential dominates the total interaction potential between NPs. As shown as in Figure 12, when two NPs collide, they are permanently bound together and thereafter diffuse as a cluster. Similarly, when two clusters collide, they bond and subsequently diffuse as a larger cluster. By this model, a fractal aggregation forms and different spongelike structures are produced after aging under the different effects of halide ions.

Two parameters affect the kinetics of formation of spongelike aggregations. The NP concentration in the solution represents the spacing-filling factor contributing to the morphology of fractal aggregates. Lower NP concentrations mean a lower spacing-filling factor and formation of smaller-sized and less-compact spongelike aggregates formed. The effect of NP size is mainly reflected by the diffusion rate in solution and surface reactivity. Therefore, the kinetics of formation of spongelike structures can be tuned by controlling the concentration and size of the NPs.

CONCLUSIONS

In summary, we have demonstrated a facile approach for template-free and environmentally friendly synthesis of spongelike gold structures by halide-induced aggregation of AuNPs. The different effects of halide ions on AuNPs determined the different aggregation and fusion of AuNPs and eventually the formation of different spongelike structures. The different affinity of halide ions for AuNPs plays an important role in controlling the formation process of spongelike gold. A noticeable red-shift in the LSPR peak was found after Br^- and I^- ion treatment of AuNPs, which indicates the adsorption of the halide atoms or ions on the AuNPs. The dynamic light scattering measurements showed that the surface potentials of AuNPs varied by treatment with different types of halide, which indicates that different halide ions have different effects on the AuNPs. The halide-induced formation of spongelike gold has potential applications in catalysis and surface-enhanced Raman scattering, as well as biological detection.

ASSOCIATED CONTENT

Supporting Information

Additional figures as described in the text, including EDX spectrum of spongelike structures and SEM images of assemblies of AuNPs. This material is available free of charge via the Internet at http://pubs.acs.org.

AUTHOR INFORMATION

Corresponding Author

*E-mail: zhangzhiq2010@hotmail.com.

Notes

The authors declare no competing financial interest.

ACKNOWLEDGMENTS

This work was supported by grant from the National Natural Science Foundation of China (no. 11034007 and no. 61102023) and by a grant from the National High Technology

Research and Development Program of China (863 Program) (no. 2012AA040503).

REFERENCES

(1) Erlebacher, J.; Aziz, M. J.; Karma, A.; Dimitrov, N.; Sieradzki, K. Evolution of Nanoporosity in Dealloying. *Nature* **2001**, *410*, 450−453.

(2) Zielasek, V.; Jürgens, B.; Schulz, C.; Biener, J.; Biener, M. M.; Hamza, A. V.; Bäumer, M. Gold Catalysts: Nanoporous Gold Foams. *Angew. Chem., Int. Ed.* **2006**, *45*, 8241−8244.

(3) Xu, C.; Su, J.; Xu, X.; Liu, P.; Zhao, H.; Tian, F.; Ding, Y.; Low Temperature, C. O. Oxidation over Unsupported Nanoporous Gold. *J. Am. Chem. Soc.* **2006**, *129*, 42−43.

(4) Asao, N.; Ishikawa, Y.; Hatakeyama, N.; Yamamoto, Y.; Chen, M.; Zhang, W.; Inoue, A. Nanostructured Materials as Catalysts: Nanoporous-Gold-Catalyzed Oxidation of Organosilanes with Water. *Angew. Chem., Int. Ed.* **2010**, *49*, 10093−10095.

(5) Wittstock, A.; Wichmann, A.; Bäumer, M. Nanoporous Gold as a Platform for a Building Block Catalyst. *ACS Catal.* **2012**, *2*, 2199−2215.

(6) Fujita, T.; Guan, P.; McKenna, K.; Lang, X.; Hirata, A.; Zhang, L.; Tokunaga, T.; Arai, S.; Yamamoto, Y.; Tanaka, N.; Ishikawa, Y.; Asao, N.; Yamamoto, Y.; Erlebacher, J.; Chen, M. Atomic Origins of the High Catalytic Activity of Nanoporous Gold. *Nat. Mater.* **2012**, *11*, 775−780.

(7) Wittstock, A.; Zielasek, V.; Biener, J.; Friend, C.; Bäumer, M. Nanoporous Gold Catalysts for Selective Gas-Phase Oxidative Coupling of Methanol at Low Temperature. *Science* **2010**, *327*, 319−322.

(8) Yu, Y.; Gu, L.; Lang, X.; Zhu, C.; Fujita, T.; Chen, M.; Maier, J. Li Storage in 3D Nanoporous Au-Supported Nanocrystalline Tin. *Adv. Mater.* **2011**, *23*, 2443−2447.

(9) Ding, Y.; Chen, M.; Erlebacher, J. Metallic Mesoporous Nanocomposites for Electrocatalysis. *J. Am. Chem. Soc.* **2004**, *126*, 6876−6877.

(10) Zeis, R.; Mathur, A.; Fritz, G.; Lee, J.; Erlebacher, J. Platinum-Plated Nanoporous Gold: An Efficient, Low Pt Loading Electrocatalyst for PEM Fuel Cells. *J. Power Sources* **2007**, *165*, 65−72.

(11) Jia, F.; Yu, C.; Ai, Z.; Zhang, L. Fabrication of Nanoporous Gold Film Electrodes with Ultrahigh Surface Area and Electrochemical Activity. *Chem. Mater.* **2007**, *19*, 3648−3653.

(12) Zhang, J.; Ma, H.; Zhang, D.; Liu, P.; Tian, F.; Ding, Y. Electrocatalytic Activity of Bimetallic Platinum−Gold Catalysts Fabricated Based on Nanoporous Gold. *Phys. Chem. Chem. Phys.* **2008**, *10*, 3250−3255.

(13) Lang, X.-Y.; Fu, H.-Y.; Hou, C.; Han, G.-F.; Yang, P.; Liu, Y.-B.; Jiang, Q. Nanoporous Gold Supported Cobalt Oxide Microelectrodes as High-Performance Electrochemical Biosensors. *Nat. Commun.* **2013**, *4*.

(14) Wei, Q.; Zhao, Y.; Xu, C.; Wu, D.; Cai, Y.; He, J.; Li, H.; Du, B.; Yang, M. Nanoporous Gold Film Based Immunosensor for Label-Free Detection of Cancer Biomarker. *Biosens. Bioelectron.* **2011**, *26*, 3714−3718.

(15) Biener, J.; Wittstock, A.; Zepeda-Ruiz, L.; Biener, M.; Zielasek, V.; Kramer, D.; Viswanath, R.; Weissmüller, J.; Bäumer, M.; Hamza, A. Surface-Chemistry-Driven Actuation in Nanoporous Gold. *Nat. Mater.* **2008**, *8*, 47−51.

(16) Kramer, D.; Viswanath, R. N.; Weissmüller, J. Surface-Stress Induced Macroscopic Bending of Nanoporous Gold Cantilevers. *Nano Lett.* **2004**, *4*, 793−796.

(17) Forty, A. Corrosion Micromorphology of Noble Metal Alloys and Depletion Gilding. 1979.

(18) Pickering, H.; Swann, P. Electron Metallography of Chemical Attack upon Some Alloys Susceptible to Stress Corrosion Cracking. *Corrosion* **1963**, *19*, 373t−389t.

(19) Forty, A.; Durkin, P. A Micromorphological Study of the Dissolution of Silver−Gold Alloys in Nitric Acid. *Philos. Mag. A* **1980**, *42*, 295−318.

(20) Moffat, T. P.; Fan, F. R. F.; Bard, A. J. Electrochemical and Scanning Tunneling Microscopic Study of Dealloying of Cu_3Au. *J. Electrochem. Soc.* **1991**, *138*, 3224−3235.

(21) Chen, S.; Sanz, F.; Ogletree, D.; Hallmark, V.; Devine, T.; Salmeron, M. Selective Dissolution of Copper from Au-Rich Cu−Au Alloys: An Electro Chemical STM Study. *Surf. Sci.* **1993**, *292*, 289−297.

(22) Zhang, Q.; Zhang, Z. On the Electrochemical Dealloying of Al-Based Alloys in a NaCl Aqueous Solution. *Phys. Chem. Chem. Phys.* **2010**, *12*, 1453−1472.

(23) Walsh, D.; Arcelli, L.; Ikoma, T.; Tanaka, J.; Mann, S. Dextran Templating for the Synthesis of Metallic and Metal Oxide Sponges. *Nat. Mater.* **2003**, *2*, 386−390.

(24) Zhang, H.; Hussain, I.; Brust, M.; Cooper, A. I. Emulsion-Templated Gold Beads Using Gold Nanoparticles as Building Blocks. *Adv. Mater.* **2004**, *16*, 27−30.

(25) Wang, D.; Luo, H.; Kou, R.; Gil, M. P.; Xiao, S.; Golub, V. O.; Yang, Z.; Brinker, C. J.; Lu, Y. A General Route to Macroscopic Hierarchical 3D Nanowire Networks. *Angew. Chem., Int. Ed.* **2004**, *116*, 6295−6299.

(26) Sun, S.; Wu, P. Easy Fabrication of Macroporous Gold Films Using Graphene Sheets as a Template. *ACS Appl. Mater. Interfaces* **2013**, *5*, 3481−3486.

(27) Balogh, D.; Tel-Vered, R.; Freeman, R.; Willner, I. Photochemically and Electrochemically Triggered Au Nanoparticles "Sponges". *J. Am. Chem. Soc.* **2011**, *133*, 6533−6536.

(28) Frasconi, M.; Tel-Vered, R.; Riskin, M.; Willner, I. Surface Plasmon Resonance Analysis of Antibiotics Using Imprinted Boronic Acid-Functionalized Au Nanoparticle Composites. *Anal. Chem.* **2010**, *82*, 2512−2519.

(29) Balogh, D.; Tel-Vered, R.; Riskin, M.; Orbach, R.; Willner, I. Electrified Au Nanoparticle Sponges with Controlled Hydrophilic/Hydrophobic Properties. *ACS Nano* **2010**, *5*, 299−306.

(30) Riskin, M.; Tel-Vered, R.; Lioubashevski, O.; Willner, I. Ultrasensitive Surface Plasmon Resonance Detection of Trinitrotoluene by a Bis-aniline−Cross-Linked Au Nanoparticles Composite. *J. Am. Chem. Soc.* **2009**, *131*, 7368−7378.

(31) Qin, G. W.; Liu, J.; Balaji, T.; Xu, X.; Matsunaga, H.; Hakuta, Y.; Zuo, L.; Raveendran, P. A Facile and Template-Free Method To Prepare Mesoporous Gold Sponge and Its Pore Size Control. *J. Phys. Chem. C* **2008**, *112*, 10352−10358.

(32) Gao, S.; Zhang, H.; Wang, X.; Yang, J.; Zhou, L.; Peng, C.; Sun, D.; Li, M. Unique Gold Sponges: Biopolymer-Assisted Hydrothermal Synthesis and Potential Application as Surface-Enhanced Raman Scattering Substrates. *Nanotechnology* **2005**, *16*, 2530.

(33) Liu, R.; Liu, J.-f.; Zhou, X.-x.; Sun, M.-T.; Jiang, G.-b. Fabrication of a Au Nanoporous Film by Self-Organization of Networked Ultrathin Nanowires and Its Application as a Surface-Enhanced Raman Scattering Substrate for Single-Molecule Detection. *Anal. Chem.* **2011**, *83*, 9131−9137.

(34) Klajn, R.; Gray, T. P.; Wesson, P. J.; Myers, B. D.; Dravid, V. P.; Smoukov, S. K.; Grzybowski, B. A. Bulk Synthesis and Surface Patterning of Nanoporous Metals and Alloys from Supraspherical Nanoparticle Aggregates. *Adv. Funct. Mater.* **2008**, *18*, 2763−2769.

(35) Magnussen, O. Ordered Anion Adlayers on Metal Electrode Surfaces. *Chem. Rev.* **2002**, *102*, 679−726.

(36) Wasileski, S. A.; Weaver, M. J. Electrode Potential-Dependent Anion Chemisorption and Surface Bond Polarization As Assessed by Density Functional Theory. *J. Phys. Chem. B* **2002**, *106*, 4782−4788.

(37) Ocko, B. M.; Watson, G. M.; Wang, J. Structure and Electrocompression of Electrodeposited Iodine Monolayers on Gold (111). *J. Phys. Chem.* **1994**, *98*, 897−906.

(38) Magnussen, O. M.; Ocko, B. M.; Wang, J. X.; Adzic, R. R. In-Situ X-ray Diffraction and STM Studies of Bromide Adsorption on Au(111) Electrodes. *J. Phys. Chem.* **1996**, *100*, 5500−5508.

(39) Langille, M. R.; Personick, M. L.; Zhang, J.; Mirkin, C. A. Defining Rules for the Shape Evolution of Gold Nanoparticles. *J. Am. Chem. Soc.* **2012**, *134*, 14542−14554.

(40) Lohse, S. E.; Burrows, N. D.; Scarabelli, L.; Liz-Marzan, L. M.; Murphy, C. J. Anisotropic Noble Metal Nanocrystal Growth: The Role of Halides. *Chem. Mater.* **2013**.
(41) Ha, T. H.; Koo, H.-J.; Chung, B. H. Shape-Controlled Syntheses of Gold Nanoprisms and Nanorods Influenced by Specific Adsorption of Halide Ions. *J. Phys. Chem. C* **2007**, *111*, 1123−1130.
(42) Cheng, W.; Dong, S.; Wang, E. Iodine-Induced Gold-Nanoparticle Fusion/Fragmentation/Aggregation and Iodine-Linked Nanostructured Assemblies on a Glass Substrate. *Angew. Chem., Int. Ed.* **2003**, *42*, 449−452.
(43) Rai, A.; Singh, A.; Ahmad, A.; Sastry, M. Role of Halide Ions and Temperature on the Morphology of Biologically Synthesized Gold Nanotriangles. *Langmuir* **2006**, *22*, 736−741.
(44) Liu, Y.; Liu, L.; Guo, R. Br^--Induced Facile Fabrication of Spongelike Gold/Amino Acid Nanocomposites and Their Applications in Surface-Enhanced Raman Scattering. *Langmuir* **2010**, *26*, 13479−13485.
(45) Frens, G. Controlled Nucleation for the Regulation of the Particle Size in Monodisperse Gold Suspensions. *Nature* **1973**, *241*, 20−22.
(46) Turkevich, J.; Stevenson, P. C.; Hillier, J. A Study of the Nucleation and Growth Processes in the Synthesis of Colloidal Gold. *Discuss. Faraday Soc.* **1951**, *11*, 55−75.
(47) Zhang, Z.; Wu, Y. $NaBH_4$-Induced Assembly of Immobilized Au Nanoparticles into Chainlike Structures on a Chemically Modified Glass Surface. *Langmuir* **2011**, *27*, 9834−9842.
(48) Kim, T.; Lee, K.; Gong, M.-s.; Joo, S.-W. Control of Gold Nanoparticle Aggregates by Manipulation of Interparticle Interaction. *Langmuir* **2005**, *21*, 9524−9528.
(49) Verwey, E. J. W.; Overbeek, J. T. G. *Theory of the Stability of Lyophobic Colloids*; Dover Publications: Mineola, NY, 1999.
(50) Israelachvili, J. N. *Intermolecular and Surface Forces*, 3rd ed.; Academic Press: New York, 2011.
(51) Hunter, R. J.; White, L. R.; Chan, D. Y. *Foundations of Colloid Science*; Clarendon Press: Oxford, 1987; Vol. *1*.
(52) Liu, J.; Lu, Y. Preparation of Aptamer-Linked Gold Nanoparticle Purple Aggregates for Colorimetric Sensing of Analytes. *Nat. Protoc.* **2006**, *1*, 246−252.
(53) Zhao, W.; Chiuman, W.; Lam, J. C.; McManus, S. A.; Chen, W.; Cui, Y.; Pelton, R.; Brook, M. A.; Li, Y. DNA Aptamer Folding on Gold Nanoparticles: From Colloid Chemistry to Biosensors. *J. Am. Chem. Soc.* **2008**, *130*, 3610−3618.
(54) Wang, L.; Liu, X.; Hu, X.; Song, S.; Fan, C. Unmodified Gold Nanoparticles As a Colorimetric Probe for Potassium DNA Aptamers. *Chem. Commun.* **2006**, 3780−3782.
(55) Pei, L.; Mori, K.; Adachi, M. Formation Process of Two-Dimensional Networked Gold Nanowires by Citrate Reduction of $AuCl_4^-$ and the Shape Stabilization. *Langmuir* **2004**, *20*, 7837−7843.
(56) Willets, K. A.; Van Duyne, R. P. Localized Surface Plasmon Resonance Spectroscopy and Sensing. *Annu. Rev. Phys. Chem.* **2007**, *58*, 267−297.
(57) Ghosh, S. K.; Pal, T. Interparticle Coupling Effect on the Surface Plasmon Resonance of Gold Nanoparticles: From Theory to Applications. *Chem. Rev.* **2007**, *107*, 4797−4862.
(58) Jain, P. K.; El-Sayed, M. A. Noble Metal Nanoparticle Pairs: Effect of Medium for Enhanced Nanosensing. *Nano Lett.* **2008**, *8*, 4347−4352.
(59) Zhang, Z.; Wu, Y. Investigation of the $NaBH_4$-Induced Aggregation of Au Nanoparticles. *Langmuir* **2010**, *26*, 9214−9223.
(60) Finklea, H. *Electroanalytical Chemistry*; Marcel Dekker, Inc.: New York, 1996; Vol. *19*.
(61) Shipway, A. N.; Katz, E.; Willner, I. Nanoparticle Arrays on Surfaces for Electronic, Optical, And Sensor Applications. *ChemPhysChem* **2000**, *1*, 18−52.
(62) Mulvaney, P.; Pérez-Juste, J.; Giersig, M.; Liz-Marzán, L. M.; Pecharromán, C. Drastic Surface Plasmon Mode Shifts in Gold Nanorods Due to Electron Charging. *Plasmonics* **2006**, *1*, 61−66.
(63) Kielland, J. Individual Activity Coefficients of Ions in Aqueous Solutions. *J. Am. Chem. Soc.* **1937**, *59*, 1675−1678.
(64) Wang, J.; Li, Y. F.; Huang, C. Z. Identification of Iodine-Induced Morphological Transformation of Gold Nanorods. *J. Phys. Chem. C* **2008**, *112*, 11691−11695.
(65) Singh, S.; Pasricha, R.; Bhatta, U. M.; Satyam, P.; Sastry, M.; Prasad, B. Effect of Halogen Addition to Monolayer Protected Gold Nanoparticles. *J. Mater. Chem.* **2007**, *17*, 1614−1619.
(66) Poon, W. C.; Haw, M. Mesoscopic Structure Formation in Colloidal Aggregation and Gelation. *Adv. Colloid Interface Sci.* **1997**, *73*, 71−126.